The International Journal of Advanced Manufacturing Technology (2020) 111:2449–2459
https://doi.org/10.1007/s00170-020-06309-3

ORIGINAL ARTICLE

Effects of cutting parameters on roughness and residual stress of maraging steel specimens produced by additive manufacturing

A. R. Oliveira[1] · A. L. Jardini[2,3] · E. G. Del Conte[1]

Received: 10 August 2020 / Accepted: 21 October 2020 / Published online: 28 October 2020

Abstract
Additive Manufacturing of metallic parts by powder bed fusion (PBF) has great potential to build complex geometries with innovative materials in a broad field of applications; however, it also presents some limitations as residual stresses, porosities, microcracks, and high roughness that restrict your plateau of productivity. Therefore, an alternative to improve the surface condition of PBF parts is the post-processing as milling. Maraging steel 300 is an important material used in the PBF process, considering its application in different segments, like automotive, tooling, and aerospace. Although there are a few works that investigated the effects of cutting parameters on the surface condition of maraging steel 300 components produced by PBF, this work investigated the effects of different cutting speeds (v_c) and feed per tooth (f_z) on average roughness R_a and residual stress of maraging 300 specimens. The lowest roughness level of $R_a = 0.31$ μm was obtained with $f_z = 0.02$ mm/tooth and $v_c = 250$ m/min. Furthermore, the cutting speed had a relevant effect on the compressive behavior of residual stresses. The feed per tooth combined with the cutting speed improved the surface roughness and the compressive residual stress of the specimens, showing the importance of considering both these parameters in the milling process planning of PBF maraging steel parts.

Keywords Maraging steel 300 · Roughness · Residual stress · Powder bed fusion · Cutting parameters

1 Introduction

Additive manufacturing of metallic materials by powder bed fusion (PBF) characterize the fabrication of components based on the fusion of metallic powders disposed on the build platform [1–3]. This layer production occurs due to thermal energy provided by a laser beam that melts the particles to bond them, giving rise to complex shapes [1–3]. Maraging steel 300 is a notable material compatible with the PBF process, considering its application in different segments, such as automotive, tooling, and aerospace [4–7]. The prior properties of this low carbon steel are the high strength and microhardness [6, 7] due to the martensite matrix with intermetallic precipitates generated by aging treatment [4, 5, 8], which limits the mobility of dislocations on the microstructure [9].

Although the potential application of PBF technology is noticeable in the industry, the main barriers to its plateau of application are microcracks, pores, and high roughness [2, 10–15]. Also, components produced by PBF present high residual stresses that require monitoring [15, 16]. Tensile residual stress promotes crack propagations, resulting in lower mechanical strength [15, 16]. However, compressive residual stress can suppress this enlargement [15] and refine the dimension precision of additive manufacturing components [16].

Milling is one of the alternatives to post-process components fabricated with additive manufacturing because of its capacity to provide better surface quality, as mentioned by Fortunato et al. [7]. During milling, the material is removed by a rotative tool that also has a translatory motion along with the work table. Thus, cutting parameters defined as cutting speed (v_c), feed per tooth (f_z), and depth of cut (a_p) characterize the process [17]. An adequate finishing, however, will depend on the correct planning and selection of cutting parameters [18].

The study of cutting parameters can be conducted with the design of experiments (DOE) approach to guarantee robust

✉ E. G. Del Conte
erik.conte@ufabc.edu.br

[1] Federal University of ABC, Av. dos Estados, 5001, Santo André, SP 09210-580, Brazil

[2] School of Chemical Engineering, University of Campinas, Campinas, Brazil

[3] National Institute of Biofabrication (INCT-BIOFABRIS), Campinas, Brazil

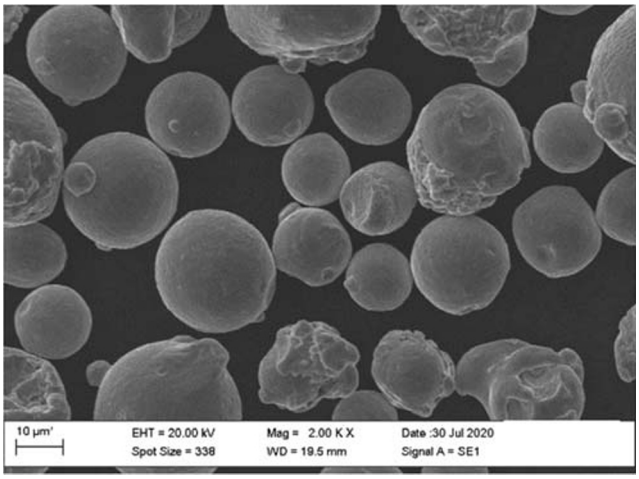

Fig. 1 Maraging steel powders

experiments. This methodology proposed by Montgomery [19] defines planning, execution, and analysis strategies to guide research and emerge as a consolidated method in literature. Lela et al. [20] examined how variations of cutting parameters in milling affect the surface roughness of steel. The most influential factors to roughness recognized were feed per tooth and cutting speed, respectively [20]. The authors also presented ways to optimize this quality feature and defined models to predict its behavior based on cutting parameters [20]. Mutua et al. [8] applied full factorial design to investigate PBF parameters and options of heat treatments to define the optimal configurations range to produce maraging steel parts.

Cutting speed increase leads to high levels of temperature, mainly, where the tool and material defined an interface [17, 21, 22]. Thus, this region assumed different behaviors during chip formation with divergent parameters [23] due to a change in mechanical responses that occurs after thermal expansion and contraction [21]. Moreover, microstructural modification induced by machining deformation [24] or a localized aging treatment [25] also influences surface finishing.

Milling parameters also influence residual stresses on the surface. Tomaz et al. [21] investigated these effects on conventional maraging steel after solution treatment. Using different flood methods, the authors found the higher effects of feed per tooth and cutting speed, respectively, on residual stress on the maraging surface [21]. Furthermore, the selection of cutting parameters also influenced the definition of compressive or tensile behavior on residual stress [21].

PBF and end milling influence the surface quality of material given the innumerous factors involved. Tan et al. [26] highlighted that the temperature gradient, different heat distribution during the laser incidence, and the cooling rate levels in the process generate a range of microstructural defects and components, such as fine and coarse cells. These PBF process characteristics can change the cutting behavior when the additively manufactured material is submitted to milling.

Thus, the roughness evaluation of a specimen produced in both is essential to take better advantage of these technologies. Moreover, it is crucial to guarantee that residual stresses will not be compromised to achieve advantageous roughness levels, considering the relevance of compressive behavior for components surface [15, 16]. To achieve materials produced by PBF with better finishing and mechanical performance combined, this work investigated the effects of cutting speed (v_c) and feed per tooth (f_z) used during post-processing by milling of maraging steel 300 specimens manufactured by PBF for the average roughness (R_a) and residual stresses based on DOE.

2 Experimental setup

2.1 Powder bed fusion

Maraging steel 300 specimen with 32 × 32 × 10 mm was produced by PBF using EOSINT M280 (Yb-laser) machine, EOS GmbH, Munich, Germany. Figure 1 illustrates the metallic maraging steel powders supplied by LPW (Carpenter Additive), Cheshire, UK. The particle size was calculated based on the micrographs with a magnification of × 500 using the software Image J. The average powder diameter resulted in 24.3 ± 10.2 μm.

Table 1 presents the chemical composition obtained by optical emission spectroscopy of the maraging specimen. During PBF, the laser power was 170 W, hatch distance was 0.1 mm, scan speed was 1250 mm/s, and the layer thickness was 0.02 mm. The nitrogen gas was used inside the chamber, and the laser performed a linear scan strategy with 67° rotation between layers.

2.2 Characterization methods

Microstructural analysis of the as-built specimen was conducted with an optical microscope Scope A1 AxioCam iCc 5 Zeiss (Jena, Germany). A prior microscopy observation of the as-

Table 1 Maraging steel chemical composition

Elements	Ni	Co	Mo	Ti	Al	Cr	Si	Mn	C	N	P	S	Fe
% weight	19.00	9.36	4.54	1.00	0.038	0.02	0.07	0.04	0.024	0.017	0.009	< 0.001	bal.

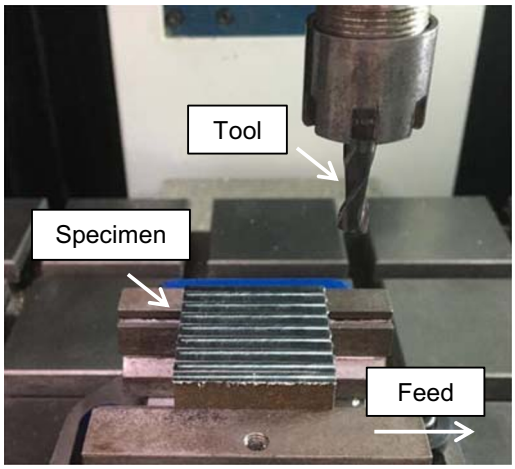

Fig. 2 Milling conditions for experiments

built specimen surface investigated the pattern provided by PBF, especially in terms of high roughness sources. After the polishing and etching, both transversal and top views of the specimen surface were observed for defects' inspection.

Specimen density was measured using the Archimedes' principle, as discussed by ASTM [27]. By this approach, the specimen had the weight measure using an analytical balance and then was immersed in a water container ($\rho_{water} = 0.9982$ g/cm^3) to identify the specimen density. This method is widely applied in the literature to provide density measures of parts produced by selective laser melting (SLM) [4, 26, 28, 29].

Three tensile tests were conducted for dog-bone maraging steel 300 specimens with an XZ orientation [1] using a universal machine INSTRON 3369 of Instron, Massachusetts, USA. It was considered a load speed of 1 mm/min for the dog-bone specimens with an overall length of 60 mm, a gauge length of 14 mm, and a thickness of 2.4 mm [30]. Vickers microhardness was also measured using a microhardness tester Homis HV 1000. A 4.9 N test force was applied for 15 s. Five micro indentations were performed for the average value determination [31]. The indentations' positioning had four measurements near to the face corners and one in the center of the specimen surface. For the milled specimens' microhardness, the measurements were distributed in the center of the channel.

2.3 Milling

The post-processing was conducted in a CNC machining center Mi 136 II, CNC Group (Santa Barbara D'Oeste, Brazil),

Table 2 Cutting parameters for the milling experiments

Runs	f_z [mm/tooth]	v_c [m/min]	a_p [mm]	Spindle speed [rpm]	Feed rate [mm/min]
#1	0.08	350	0.10	18,550	2968
#2	0.08	350	0.10	18,550	2968
#3	0.02	250	0.10	13,250	530
#4	0.08	250	0.10	13,250	2120
#5	0.08	150	0.10	7950	1272
#6	0.08	250	0.10	13,250	2120
#7	0.02	250	0.10	13,250	530
#8	0.02	150	0.10	7950	318
#9	0.08	150	0.10	7950	1272
#10	0.08	250	0.10	13,250	2120
#11	0.02	150	0.10	7950	318
#12	0.08	150	0.10	7950	1272
#13	0.02	350	0.10	18,550	742
#14	0.02	150	0.10	7950	318
#15	0.02	350	0.10	18,550	742
#16	0.02	350	0.10	18,550	742
#17	0.02	250	0.10	13,250	530
#18	0.08	350	0.10	18,550	2968

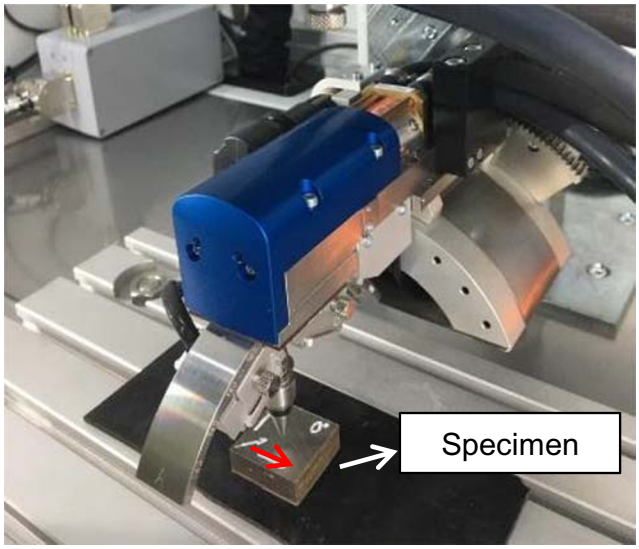

Fig. 3 Residual stress evaluation. Red arrow shows the measurement direction

using two-flute end mill tools model S902 with Ø6 mm, Dormer (Šumperk, Czech Republic). The tools were made from cemented carbide with helix angle $\lambda = 30°$. The depth of cut (ap) of 0.1 mm was kept constant [7, 32]. This process followed the DOE, considering two factors v_c and f_z with three and two levels, respectively. Using the full factorial approach with three repetitions, 18 tests were performed with the configurations shown in Fig. 2 and Table 2. The selection of the v_c and the f_z levels followed prior studies and the literature [7, 21, 32].

Roughness was measured five times for each specimen, centralized in the channel of the test areas and following the feed direction, by a roughness tester Surtronic S-218 Taylor Hobson (Leicester, UK). Considering a Gaussian filter, the cutoff parameter of 0.8 mm provided the average roughness (R_a) of each specimen. Top surface as-built roughness was also performed for comparison using the same measurement direction. Statistical analysis application enabled the investigation of the effects of milling parameters on the roughness using the software Action Stat (Sao Carlos, Brazil).

The surface finishing of the machined areas was also examined using the optical microscope and under the scanning electron microscope (SEM) Fei Quanta 250, Thermo Fisher Scientific (Massachusetts, USA). At last, residual stresses of the as-built and milled specimens were measured by X-ray diffraction with a Cr-kα tube, a voltage of 25 kV, and a current of 7 mA using the Stresstech G2R machine (Rennerod, Germany). The measurements followed the same direction used for the roughness evaluation, which was also the feed direction, as shown in Fig. 3.

3 Results and discussion

3.1 PBF manufactured specimens characterization

As shown in Fig. 4, the building orientation used (XY) provides a better finishing for the top of the specimen due to the remelting conducted for the last three layers. This process consists of carrying out a second laser beam incidence above the material to melt this region again in PBF [33, 34]. The roughness drops 68% on the remelted face when compared to the side face (Fig. 4). Thus, the remelted face (top) was considered for the specimen characterization due to a better roughness condition for material applications.

One of the most important specifications of the PBF process for surface characteristics and quality is the laser energy density, especially because of its dependence on other relevant parameters [2]. The relation involving scan speed (v), laser power (P), and hatch distance (h), in which the laser energy density (E_d) can be determined, is expressed by Eq. 1 [14]. The laser energy density per volume (E_{dvol}) can be calculated when the layer thickness (t) is included in the denominator [6, 8, 26].

$$E_d = \frac{P}{vh} \quad \left[\frac{J}{mm^2}\right] \tag{1}$$

In this study, an energy density $E_d = 1.36$ J/mm^2 and $E_{dvol} = 68.00$ J/mm^3 were used. These values of energy density can provide low porosities levels according to other studies [8, 26], because of a nearly fully dense structure achieved for maraging steel. This characteristic was also identified in this study based on the relative density of $99.47 \pm 0.04\%$.

Mutua et al. [8] also verified a high-quality surface when a laser energy density per volume of 71.43 J/mm^3 was used. Thus, the $E_{dvol} = 68.00$ J/mm^3 adopted in this study had a great

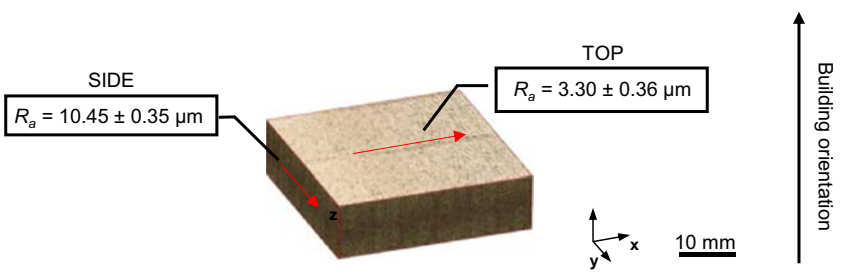

Fig. 4 Roughness of different faces of maraging steel specimen. Red arrows show the average roughness measurement directions

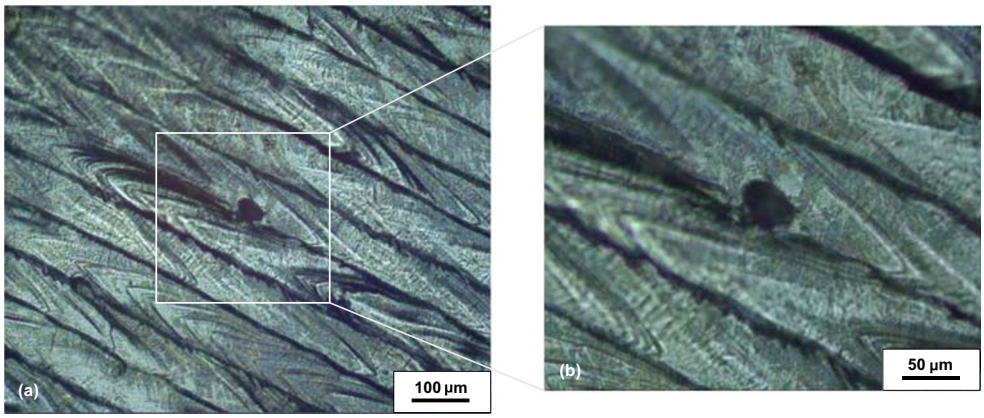

Fig. 5 **a** Surface of the as-built condition and **b** an unmelted powder identified on the surface

potential to provide low surface roughness. Few spherical elements stayed along the remelted as-built surface, as shown in Fig. 5a. These units are the remaining metallic powders derived for a melting issue, considering the diameter of ≈ Ø 40 µm (Fig.5b).

The as-built condition presented few defects inherent to PBF, especially melting flaws and a rough aspect with an average roughness of $R_a = 3.30 \pm 0.36$ µm. After metallography preparation and etching, it could be observed a characteristic microstructure of maraging steel 300 produced by PBF. Figure 6a shows the semielliptical melt pools [8, 28] with some interior pores spread in the specimen, even with the high density measured. Moreover, the superior view of the specimen, in which the evaluation of the average roughness and residual stress took place, presented the rotational scan strategy adopted for the process with 67° between consecutive layers (Fig. 6b).

Figure 7 shows the stress-strain diagram of a tensile test conducted on the as-built specimens. Based on the three repetitions performed, the average ultimate tensile stress (UTS) was 1047.8 ± 56.9 MPa, and the elongation at break was 18.2 ± 1.2%. All the parameters analyzed confirmed the high mechanical properties of maraging steel 300 specimens manufactured by PBF, especially the high ductility, considering the high elongation at break and the diagram shape [1] (Fig. 7).

3.2 Milled specimens

3.2.1 Roughness

The analysis of variance of roughness results identified two outliers (runs 12 and 18) based on the standardized and studentized residuals analysis, considering that both values

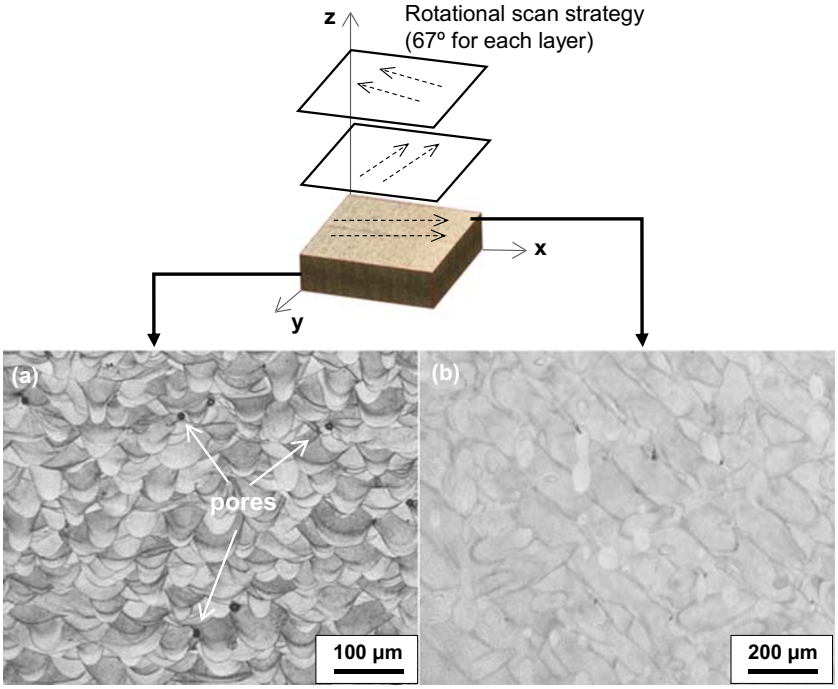

Fig. 6 Microstructure of (**a**) build-oriented face (side) and (**b**) superior view of maraging steel 300 as-built specimen

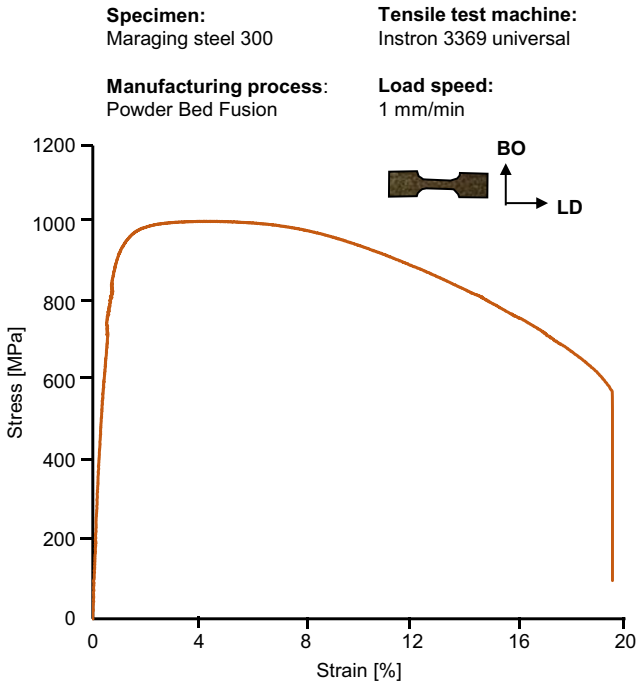

Fig. 7 Stress vs. strain diagram of maraging steel 300 produced by PBF. BO refers to the specimen building orientation, whereas LD refers to the loading direction during the tensile tests

exceeded the acceptable interval from −3 to 3 [19]. Residuals reflect the differences between the experimental values and the fitted data [19]. Thus, both measures were disregarded for further investigations. Table 3 presents the values provided by the final evaluation using ANOVA [19]. Considering a significance level of 0.05, feed per tooth and cutting speed were significant for average roughness on the surface, with the p values of 0.000 and 0.007, respectively. Also, statistic F exhibited the same relation and emphasized the major effect of feed per tooth on roughness. The main effects' graphs show these behaviors (Fig. 8). The predominant effect of f_z was also highlighted in other studies [20, 21].

In the case of the cutting speed effect, a smooth decline on roughness (~0.1 μm) occurred when v_c was adjusted from 150 to 250 m/min (Fig. 8). On the other hand, R_a remained almost constant at 1.4 μm between 250 and 350 mm/min. A roughness average of 0.34 μm could reach a value of 2.50 μm when feed changed from 0.02 to 0.08 mm/tooth (Fig. 8).

The chip formation mechanism involved in the additively manufactured maraging steel was shown in Fig. 9. On materials produced with conventional methods, the crack propagation is expected to occur along the cutting line, according to Hashimura et al. [35]. However, considering the melt pools configured with the laser scanning and some pores generated during the PBF process, the crack growth can suffer deviations from this pattern, following in some cases the melt pool boundaries [36] or even with the layer shearing [8] (Fig. 9). Moreover, regarding the maraging steel 300 properties, the material had a ductile behavior with high strength and elongation at break (Fig. 7), which improve its capacity to great plastically deform before fracture.

Regarding the deviations among the roughness' values observed for the 150 m/min, 250 m/min, and 350 m/min (Fig. 10), there was not a significant difference to consider when $f_z = 0.02$ mm/tooth. However, the v_c increase provided soft lower roughness when $f_z = 0.08$ mm/tooth with a range of 0.18 μm, which justified the presence of a weak v_c significance (Table 3). Fortunato et al. [7] also observed this v_c trend when $f_z = 0.08$ mm/tooth during milling of as-built additive manufactured maraging steel specimens. It was expected a roughness improvement with increasing v_c for conventional materials [17, 22, 23, 37]. Chen [37] highlighted that this mechanism could occur because of the less plastic behavior of the material when higher cutting speeds are used in machining. Due to the enhanced maraging steel capacity to plastically deform and its microstructure/chip formation interaction, this mechanism did not occur for the investigated cutting conditions.

Roughness was expected to express a growth trend when feed per tooth increased based on literature for conventional [21] and additively manufactured materials [38], and the present study reinforced this trend. Feed per tooth could significantly (Table 3) reduce the roughness when considering the lower level (0.02 mm/tooth) for all cutting speeds, as shown in Fig. 10. The milling-induced changes on microstructure [24, 39] also could explain the differences for both f_z results. The interaction between v_c and f_z did not express statistical significance for surface roughness, considering the p value > 0.05 (Table 3). Tomaz et al. [21] found a significant interaction when investigated the conventional maraging steel after milling with lubrication, but the materials' microstructure defined with different manufacturing processes together with the different conditions of the machining could influence the difference regarding this study.

Table 3 ANOVA for surface roughness

Factor	Degrees of freedom	Sum of squares (adj.)	F statistic	p value
f_z	1	16.89	4637.33	0.000
v_c	1	0.04	10.36	0.007
f_z *v_c	1	0.00	1.23	0.288
Residuals	12	0.04		

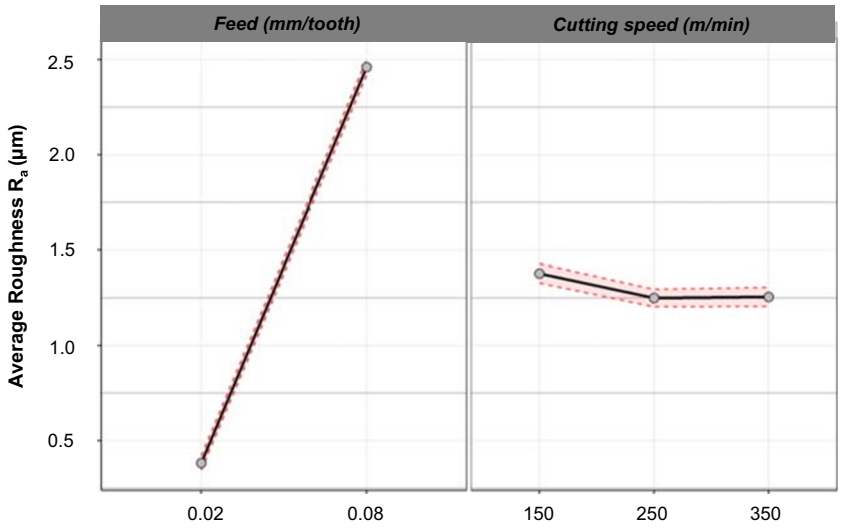

Fig. 8 Main effects' graphs of feed per tooth and cutting speed on roughness

By visual inspection, it was verified that deformed material got stuck in the surface, mainly when v_c was 250 m/min and 350 m/min. SEM images confirmed the presence of these elements (Fig. 11a and b). Microstructural heterogeneities induced by PBF could enable exceptional intense plastic deformations in some surface regions [23], which can explain these adhered elements on the surface. This occurrence in the intermediate and high cutting speeds also enlarges that the high mechanical performance of the maraging steel, as aforementioned, still presents when using these levels. The size flow phenomenon, which consists in the size smearing of materials disposed near the tool edges along with feed motion [40], was observed for all parameter combinations (Fig. 11c).

Moreover, the disparities observed among parameters were not related to vibrations, due to the absence of chatter marks [23]. Figure 12 shows the best (a) and worst (b) surface conditions obtained in the study. All conditions showed feed marks generated by feed per tooth (Fig. 9) with different intensities, as verified by Biondani et al. [40] and Jeelani and Ramakrishnan [23]. Higher f_z defined more pronounced tool marks. Additionally, milling conducted with the low levels of v_c (150 m/min) and f_z (0.02 mm/tooth) expressed a different pattern, as shown in Fig. 12c, in which microvoids were generated on the surface. Cavities are also common for low v_c during machining of conventional alloys due to the broken chip fragments, according to Jeelani and Ramakrishnan [23]. Also, the PBF effects on the cutting mechanism show the possibility of microvoid generations on the milled surface when pores are present during the chip formation (Fig. 9).

The cutting parameters combination that showed the low surface roughness was $f_z = 0.02$ mm/tooth and $v_c = 250$ m/min (Fig. 10). The drop from $R_a = 3.30 \pm 0.36$ µm of the remelted as-built condition to the optimized $R_a = 0.31 \pm 0.03$ µm enabled a reduction of 90.5% on surface roughness when the milling was performed in the better configuration among the tests. At last, one new tool was used for each machining face resulting in minimum tool wear.

3.2.2 Residual stress

Figure 13 show the residual stress measured for the milled specimens. The evaluation was done to the feed per tooth $f_z = 0.02$ mm/tooth due to the improved roughness results found for this condition.

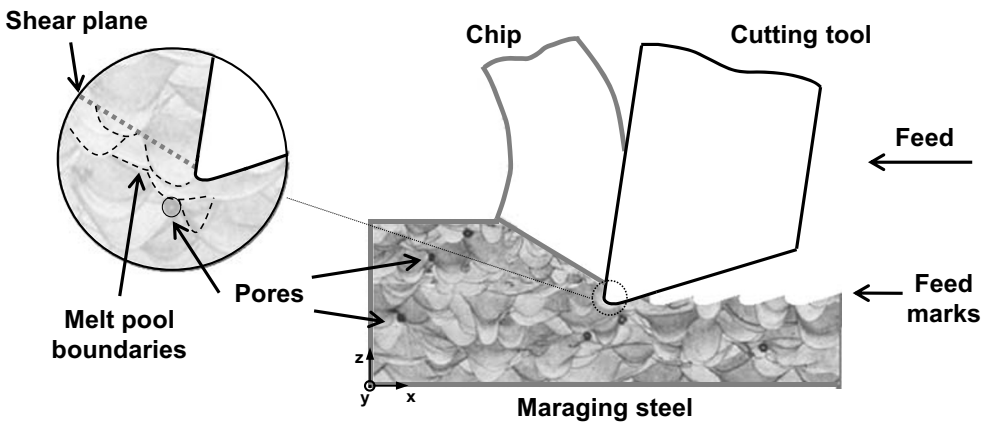

Fig. 9 Chip formation mechanism

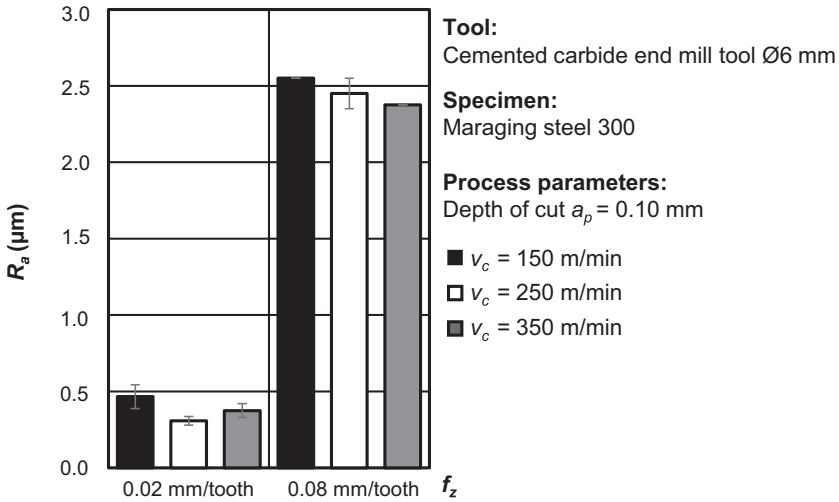

Fig. 10 Surface roughness results after milling

It is well known that the PBF process generates higher residual stresses, and mainly tensile residual stresses are observed [4, 15, 16]. Nevertheless, the remelting of the top layers induced compressive stress on the specimen. This observation could be related to the austenite-martensite transformation [16] during the PBF process. Compressive residual stresses are beneficial to mechanical properties, mainly to reduce the probability of crack open [16]. Compressive residual stresses identified for the remelted as-built specimen were reduced from − 394 ± 18 MPa to an average of − 25 ± 3 MPa, − 57 ± 8 MPa, and − 103 ± 4 MPa when performing milling the v_c 150 m/min, 250 m/min, and 350 m/min, respectively. Becker and Dimitrov [4] observed high tensile residual stresses of 720 ± 142 MPa and 455 ± 91 MPa for the single and double scan strategy, respectively. The discrepancy among the remelted and milled specimens' results was related to the surface conditions.

Higher cutting speeds defined more compressive residual stress (Fig. 13). A strong negative correlation between both variables was obtained, considering the Pearson coefficient of − 0.84. The increase of cutting speed provided more intense plastic deformations, identified with the presence of deformed materials attached on the surface [23]. This mechanism could enable the generation of less tensile residual stress when the cutting speed increased, considering the v_c range adopted [41]. Hence, the use of v_c = 250 m/min and v_c = 350 m/min for maraging steel milling showed a way to improve surface roughness taking the benefit to induce compressive residual stress on the final part.

3.2.3 Microhardness

The polished as-built specimen reached a higher level of 399 ± 10 HV. The remelted face showed an average of 329 ± 40 HV. The decrease in microhardness with the remelting followed the literature [34]. Aging heat treatment generates higher hardness for maraging steel specimens [8, 29]. Remelting of the last three layers also induces a localized aging treatment [33], but the hardening mechanism provided by this effect was less expressive based on the microhardness results. Moreover, the second laser scanning performed with the remelting can define coarser grains in the microstructure due to a different kind of heat flow and solidification time [42]. Thus, it could also induce a lower microhardness, as emphasized by Bhardwaj and Shukla [42].

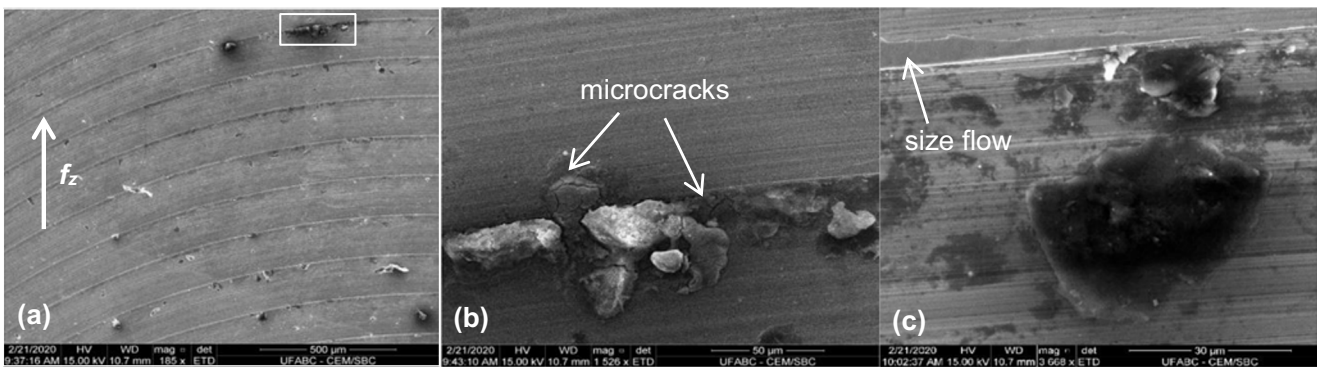

Fig. 11 SEM images of the milled maraging steel 300 emphasizing the (**a**) adhered materials, (**b**) microcracks inherent to residual elements, and (**c**) the size flow phenomenon

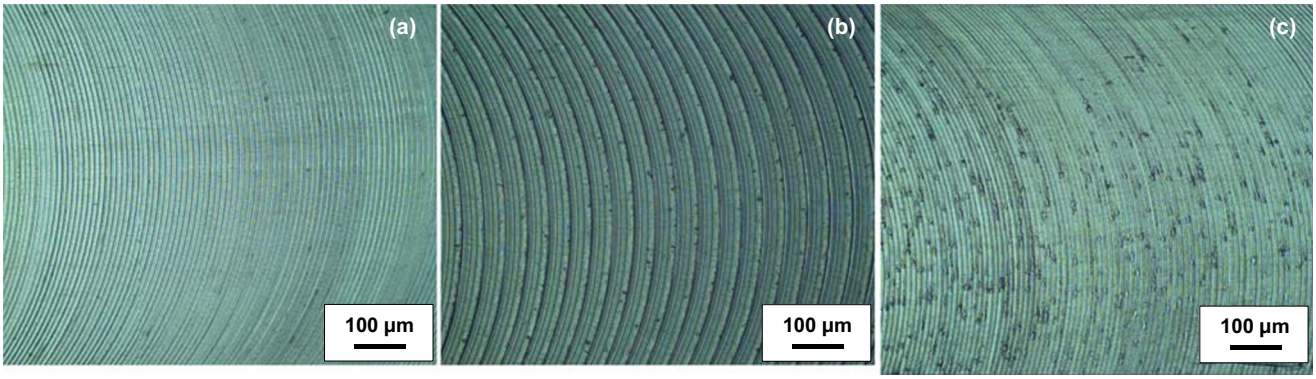

Fig. 12 Surfaces obtained for (**a**) the lower roughness (f_z = 0.02 mm/tooth and v_c = 250 m/min); (**b**) the higher roughness (f_z = 0.08 mm/tooth and v_c = 150 m/min); and (**c**) the different pattern identified for f_z = 0.02 mm/tooth and v_c = 150 m/min

The microhardness evaluation after milling was done to the f_z that had a better performance for roughness improvement (f_z = 0.02 mm/tooth). Milled specimens expressed almost the same microhardness average for the three levels of cutting speed. The results were 412 ± 9 HV, 414 ± 9 HV, and 409 ± 19 HV for v_c = 150 m/min, v_c = 250 m/min, and v_c = 350 m/min, respectively. Figure 14 presents the comparison of microhardness among all specimens. The higher deviation obtained for the remelted face in comparison to the others is related to the limitation imposed by the roughness and surface defects for microhardness evaluation in the prior [43]. Focusing on the as-built (polished) and the machined specimens, the R_a diverged approximately 0.12 µm among the milled specimens, so the impact of this factor for microhardness evaluation was disregarded.

Closer microhardness results among the three milled specimens emphasize that cutting speed did not provide the required thermal conditions for the occurrence of aging with the feed per tooth f_z = 0.02 mm/tooth. The presence of different levels of compressive residual stress on the surface before and after milling could also affect the microhardness [39]. Regarding the lower differences for the compressive residual stresses among the milled surfaces with different cutting speeds (Fig. 13), both the residual stress and the microstructural and phase changes resulted from the material plastic deformation during milling [7, 24] could influence the microhardness [39]. The latter, work hardening [39], together with the effect of the polishing, could also explain the possible smooth average microhardness increase observed for the polished to milled specimens. The lack of relation between cutting speed and surface microhardness was also evidenced by a Pearson coefficient of − 0.14.

4 Conclusion

Effects of cutting speed and feed per tooth used during milling of maraging steel 300 manufactured by PBF on the average roughness and residual stresses were investigated. The main findings emphasized the combined improvements in surface roughness and residual stresses can be achieved with adequate cutting parameters' selection. Considering the almost fully

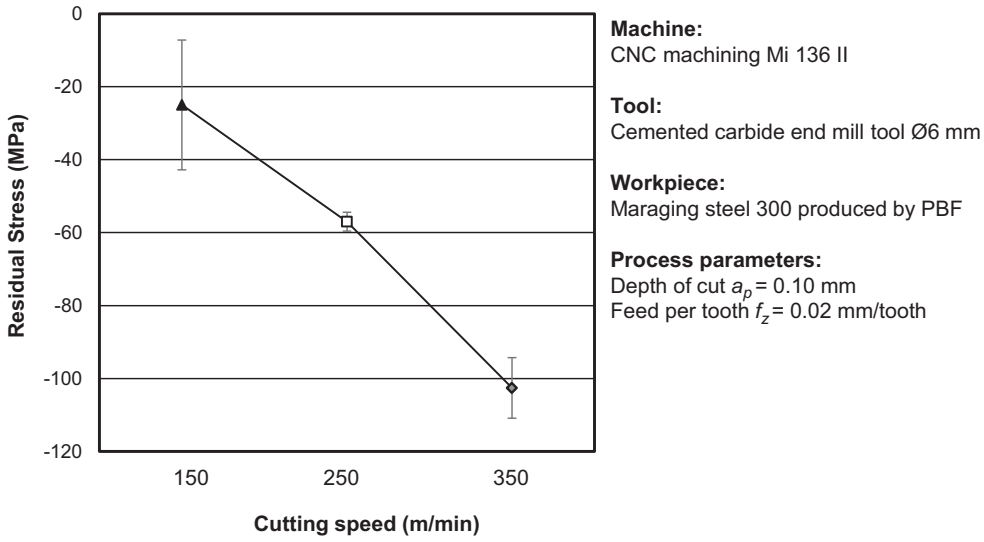

Fig. 13 Residual stress of maraging steel

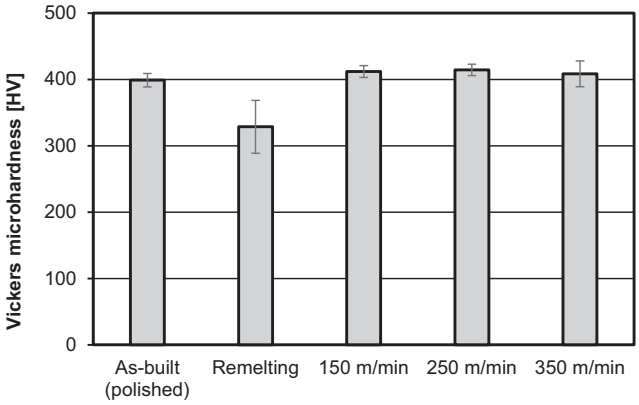

Fig. 14 Average Vickers microhardness

dense maraging steel produced by PBF, high mechanical properties could be achieved, especially the ultimate tensile stress of 1047.8 ± 56.9 MPa. Residual stresses obtained for a remelted surface showed compressive residual stress that is beneficial for maraging applications. However, roughness expressed values above 3.00 μm that needed to be enhanced.

Milling used as post-processing provided a roughness decrease from 3.30 μm (as-built) to 0.31 μm, when f_z = 0.02 mm/tooth and v_c = 250 m/min was adopted. Among f_z and v_c, feed per tooth was more significant to refine roughness levels. Cutting speed also affected roughness, but the interaction between f_z and v_c did not present statistical significance for roughness. The melt pools, layer construction, and porosity generated during the additive manufacturing can affect the chip formation.

Focusing on the best feed per tooth condition (0.02 mm/tooth), residual stress evaluation emphasized the generation of compressive residual stress for all cutting speeds used. v_c = 350 m/min resulted in the higher compressive residual stress (− 103 ± 4 MPa). The feed per tooth combined with the cutting speed improved the surface roughness and the compressive residual stress of the specimens, showing the importance of considering both these parameters in the milling process planning of PBF maraging steel parts.

Acknowledgments Special thanks are due to Henrique Lopes de Castro, Allison Denis Carros Nizes, Osmando Cardoso, and Julián Arnaldo Ávila Diaz. The authors are grateful to the Multiuser Central Facilities (UFABC) for the experimental support.

Funding Project grant #2018/11282-0, São Paulo Research Foundation (FAPESP). This study was financed in part by the Coordenação de Aperfeiçoamento de Pessoal de Nível Superior – Brasil (CAPES) – Finance Code 001.

References

1. ASTM International, 52921:2019 - Standard terminology for additive manufacturing - coordinate systems and test (2019) 1–13. https://doi.org/10.1520/F2921
2. Lou S, Jiang X, Sun W, Zeng W, Pagani L, Scott PJ (2019) Characterisation methods for powder bed fusion processed surface topography. Precis Eng 57:1–15. https://doi.org/10.1016/j.precisioneng.2018.09.007
3. Kamath C (2016) Data mining and statistical inference in selective laser melting. Int J Adv Manuf Technol 86:1659–1677. https://doi.org/10.1007/s00170-015-8289-2
4. Becker TH, Dimitrov D (2016) The achievable mechanical properties of SLM produced Maraging Steel 300 components. Rapid Prototyp J 22:487–494. https://doi.org/10.1108/RPJ-08-2014-0096
5. Jägle EA, Choi PP, Van Humbeeck J, Raabe D (2014) Precipitation and austenite reversion behavior of a maraging steel produced by selective laser melting. J Mater Res 29:2072–2079. https://doi.org/10.1557/jmr.2014.204
6. Casalino G, Campanelli SL, Contuzzi N, Ludovico AD (2015) Experimental investigation and statistical optimisation of the selective laser melting process of a maraging steel. Opt Laser Technol 65:151–158. https://doi.org/10.1016/j.optlastec.2014.07.021
7. Fortunato A, Lulaj A, Melkote S, Liverani E, Ascari A, Umbrello D (2018) Milling of maraging steel components produced by selective laser melting. Int J Adv Manuf Technol 94:1895–1902. https://doi.org/10.1007/s00170-017-0922-9
8. Mutua J, Nakata S, Onda T, Chen ZC (2018) Optimization of selective laser melting parameters and influence of post heat treatment on microstructure and mechanical properties of maraging steel. Mater Des 139:486–497. https://doi.org/10.1016/j.matdes.2017.11.042
9. Bai Y, Wang D, Yang Y, Wang H (2019) Effect of heat treatment on the microstructure and mechanical properties of maraging steel by selective laser melting. Mater Sci Eng A 760:105–117. https://doi.org/10.1016/j.msea.2019.05.115
10. Chen Z, Wu X, Tomus D, Davies CHJ (2018) Surface roughness of selective laser melted Ti-6Al-4V alloy components. Addit Manuf 21:91–103. https://doi.org/10.1016/j.addma.2018.02.009
11. Delfs P, Tows M, Schmid HJ (2016) Optimized build orientation of additive manufactured parts for improved surface quality and build time. Addit Manuf 12:314–320. https://doi.org/10.1016/j.addma.2016.06.003
12. Promoppatum P, Yao SC (2019) Analytical evaluation of defect generation for selective laser melting of metals. Int J Adv Manuf Technol 103:1185–1198. https://doi.org/10.1007/s00170-019-03500-z
13. Bai Y, Yang Y, Xiao Z, Wang D (2018) Selective laser melting of maraging steel: mechanical properties development and its application in mold. Rapid Prototyp J 24:623–629. https://doi.org/10.1108/RPJ-05-2017-0104
14. Mohammadi M, Asgari H (2018) Achieving low surface roughness AlSi10Mg_200C parts using direct metal laser sintering. Addit Manuf 20:23–32. https://doi.org/10.1016/j.addma.2017.12.012
15. Mercelis P, Kruth JP (2006) Residual stresses in selective laser sintering and selective laser melting. Rapid Prototyp J 12:254–265. https://doi.org/10.1108/13552540610707013
16. Bhardwaj T, Shukla M (2018) Effect of laser scanning strategies on texture, physical and mechanical properties of laser sintered maraging steel. Mater Sci Eng A 734:102–109. https://doi.org/10.1016/j.msea.2018.07.089
17. Groover MP (2010) Fundamentals of modern manufacturing - materials, processes, and systems, 4th edn. Wiley, Hoboken
18. Lu C (2008) Study on prediction of surface quality in machining process. J Mater Process Technol 205:439–450. https://doi.org/10.1016/j.jmatprotec.2007.11.270
19. Montgomery DC (2008) Design and analysis of experiments, 7th edn. Wiley, Hoboken
20. Lela B, Bajić D, Jozić S (2009) Regression analysis, support vector machines, and Bayesian neural network approaches to modeling

surface roughness in face milling. Int J Adv Manuf Technol 42: 1082–1088. https://doi.org/10.1007/s00170-008-1678-z
21. Tomaz ÍV, Pardal JM, Fonseca MC (2019) Influence of minimum quantity lubrication in the surface quality of milled maraging steel. Int J Adv Manuf Technol 104:4301–4311. https://doi.org/10.1007/s00170-019-04262-4
22. Lalwani DI, Mehta NK, Jain PK (2008) Experimental investigations of cutting parameters influence on cutting forces and surface roughness in finish hard turning of MDN250 steel. J Mater Process Technol 206:167–179. https://doi.org/10.1016/j.jmatprotec.2007.12.018
23. Jeelani S, Ramakrishnan K (1985) Surface damage in machining titanium 6Al-2Sn-4Zr-2Mo alloy. J Mater Sci 20:3245–3252. https://doi.org/10.1007/BF00545191
24. Habiby F, Siddiqui TN, Hussain H, Khan MA, ul Haq A, Khan AQ (1992) Machine-induced phase transformation in a maraging steel. Mater Sci Eng A 159:261–265. https://doi.org/10.1016/0921-5093(92)90297-E
25. ASM International, ASM Handbook - Heat Treating (1991). https://doi.org/10.1016/S0026-0576(03)90166-8
26. Tan C, Zhou K, Kuang M, Ma W, Kuang T (2018) Microstructural characterization and properties of selective laser melted maraging steel with different build directions. Sci Technol Adv Mater 19: 746–758. https://doi.org/10.1080/14686996.2018.1527645
27. ASTM International, B962–13 - Standard test methods for density of compacted or sintered powder metallurgy (PM) products using Archimedes' principle (2013) 1–7. https://doi.org/10.1520/B0962-13.2
28. Yin S, Chen C, Yan X, Feng X, Jenkins R, O'Reilly P, Liu M, Li H, Lupoi R (2018) The influence of aging temperature and aging time on the mechanical and tribological properties of selective laser melted maraging 18Ni-300 steel. Addit Manuf 22:592–600. https://doi.org/10.1016/j.addma.2018.06.005
29. Conde FF, Escobar JD, Oliveira JP, Béreš M, Jardini AL, Bose WW, Avila JA (2019) Effect of thermal cycling and aging stages on the microstructure and bending strength of a selective laser melted 300-grade maraging steel. Mater Sci Eng A 758:192–201. https://doi.org/10.1016/j.msea.2019.03.129
30. ASTM International, E8/E8M Standard test methods for tension testing of metallic materials, Annu. B. ASTM Stand. 4. (2010) 1–27. https://doi.org/10.1520/E0008
31. ASTM International, E92–16: Standard test methods for Vickers hardness and Knoop hardness of metallic materials, 2016
32. Morel C, Cioca VV, Lavernhe S, Jardini AL, Conte E (2018) Part surface roughness on laser sintering and milling of maraging steel 300. 14th International Conference on High Speed Manufacturing, San-Sebastian, Spain. hal-01773243
33. Kempen K, Yasa E, Thijs L, Kruth JP, Van Humbeeck J (2011) Microstructure and mechanical properties of selective laser melted 18Ni-300 steel. Phys Procedia 12:255–263. https://doi.org/10.1016/j.phpro.2011.03.033
34. Demir AG, Previtali B (2017) Investigation of remelting and preheating in SLM of 18Ni300 maraging steel as corrective and preventive measures for porosity reduction. Int J Adv Manuf Technol 93:2697–2709. https://doi.org/10.1007/s00170-017-0697-z
35. Hashimura M, Chang YP, Dornfeld D (1999) Analysis of burr formation mechanism in orthogonal cutting. J Manuf Sci Eng Trans ASME 121:1–7. https://doi.org/10.1115/1.2830569
36. Maconachie T, Leary M, Zhang J, Medvedev A, Sarker A, Ruan D, Lu G, Faruque O, Brandt M (2020) Effect of build orientation on the quasi-static and dynamic response of SLM AlSi10Mg. Mater Sci Eng A 788. https://doi.org/10.1016/j.msea.2020.139445
37. Chen W (2000) Cutting forces and surface finish when machining medium hardness steel using CBN tools. Int J Mach Tools Manuf 40:455–466. https://doi.org/10.1016/S0890-6955(99)00011-5
38. Kaynak Y, Tascioglu E (2018) Finish machining-induced surface roughness, microhardness and XRD analysis of selective laser melted Inconel 718 alloy. Procedia CIRP 71:500–504. https://doi.org/10.1016/j.procir.2018.05.013
39. Du W, Bai Q, Zhang B (2018) Machining characteristics of 18Ni-300 steel in additive/subtractive hybrid manufacturing. Int J Adv Manuf Technol 95:2509–2519. https://doi.org/10.1007/s00170-017-1364-0
40. Biondani F, Bissacco G, Hansen HN (2020) Surface topography analysis of ball end milled tool steel surfaces. Procedia CIRP. 87: 153–158. https://doi.org/10.1016/j.procir.2020.03.002
41. Navas VG, Gonzalo O, Bengoetxea I (2012) Effect of cutting parameters in the surface residual stresses generated by turning in AISI 4340 steel. Int J Mach Tools Manuf 61:48–57. https://doi.org/10.1016/j.ijmachtools.2012.05.008
42. Bhardwaj T, Shukla M (2018) Direct metal laser sintering of maraging steel: effect of building orientation on surface roughness and microhardness. Mater Today Proc 5:20485–20491. https://doi.org/10.1016/j.matpr.2018.06.425
43. Callister WD (2001) Fundamentals of materials science and engineering. Wiley, Hoboken